

Shape resonances in nested diffraction gratings

Angela N. Fantino¹, Susana I. Grosz² and Diana C. Skigin¹,
Grupo de Electromagnetismo Aplicado,
Departamento de Física,
Facultad de Ciencias Exactas y Naturales,
Universidad de Buenos Aires,
Ciudad Universitaria, Pabellón I,
C1428EHA Buenos Aires, Argentina
dcs@df.uba.ar

Abstract

The diffraction problem of a plane wave impinging on a grating formed by nested cavities is solved by means of the modal method, for s and p polarization modes. The cavities are formed by perfectly conducting sheets that describe rectangular profiles. The electromagnetic response of the grating is analyzed, paying particular attention to the generation of resonances within the structure. The dependence of the resonances on the geometrical parameters of the grating is studied, and results of far and near field are shown. The results are checked and compared with those available in the literature for certain limit cases.

Keywords: surface-shape resonances, diffraction, gratings

¹Member of CONICET

²Ciclo Básico Común, Universidad de Buenos Aires

1 Introduction

Current radio detection and ranging (RADAR) technologies employ highly concentrated beams of electromagnetic energy to scan an area. The return echo is then processed to detect all targets of interest [1]. To prevent this kind of detection, a target can either deflect the beam in a direction away from the observer, absorb the energy of the incoming beam or alter the return echo by changing its frequency or shape. Giving an aircraft textured skin that could interact with an incoming beam adaptively would allow most shapes to be metamorphic to radar. Recent research based on sub-wavelength, narrow-band, resonant, corrugated, high impedance surfaces have shown promising results in this area [2, 3]. However, the speed, bandwidth and adaptability of these surfaces are limited. To avoid the narrow-band resonant behavior, lumped structures can be replaced by broadband antenna arrays that add a controlled phase delay to the reflected signal allowing beam steering away from the observer [4]. Fractal planar antennas [5]-[7] exhibit multi-band behavior and are small in electrical size, but their scattering behavior is not widely understood. Nested multilayer corrugated surfaces constitute an interesting alternative for this purpose. If successful, unwanted radiation due to finite ground planes can be minimized and the inter elemental coupling can be reduced, thus obtaining the desired effect. The study of the electromagnetic response of the two-layer periodic structure proposed in this paper is expected to provide a first approach to the behavior of multilayer surfaces and their advantages as part of broadband antennas.

The resonant behavior of infinitely periodic gratings of rectangular profile was studied by many authors, in particular for s polarization [8]-[13]. The excitation of surface shape resonances in structures comprising cavities have been lately studied for particular profiles of the corrugation. The resonant features of an isolated cavity or groove of univalued and multivalued geometries have been investigated by means of different implementations of two basic approaches: the integral and the modal methods [14]-[21]. The results show that a strong intensification inside the cavity is found for certain wavelengths when its profile is bivalued, such as a slotted cylinder or a bottle-shaped groove [18]-[20]. The effect produced by the surface shape resonances on the response of an array of cavities has also been studied [21]-[23].

The modal method employed here to solve the diffraction problem from an infinite grating comprising rectangular grooves and bottle-shaped cavities, was first formulated to deal with

simple geometries such as rectangular [9], triangular [24] or semicircular [25]. Later it was generalized for arbitrary shapes of the grooves [26, 27], and recently it was also applied to bottle-shaped cavities [21]. The implementation of the modal method for perfectly conducting structures results in a simple and efficient way of calculating the external and the internal fields, without the need of any sophisticated algorithm.

The purpose of this paper is to analyze the electromagnetic response of a two-layer perfectly-conducting grating comprising grooves and cavities. Particular attention is paid to the resonant behavior of this structure and its effect in the field distribution inside and far from the corrugations. The study of such gratings constitutes a first approach to the analysis of N-layer fractal gratings, which are expected to be useful for the control of the phase delay in the scattering response of broadband microwave antennas.

In Sec. 2 we pose the problem and give the details of the modal method applied to the present structure, for both fundamental polarization modes. In Sec. 3 we give numerical results for the reflected efficiency as well as for the near field. We analyze the dependence of the resonances on the geometrical parameters of the structure, and compare the results obtained in limit cases with those found in the literature. Finally, some conclusions are summarized in Sec. 4.

2 Theoretical formulation

We consider the diffraction of a plane wave by a two-layer nested grating. The structure is one-dimensional and infinitely periodic, and each period is formed by a bottle-shaped cavity and rectangular grooves, bounded by perfectly conducting sheets (see Fig. 1).

The wavelength of the incoming wave is λ and the angle of incidence is θ_0 . Since the structure and the fields are invariant under translations in the \hat{z} direction, the problem can be separated into two scalar problems corresponding to the basic modes of polarization: s (electric field parallel to the rulings) and p (magnetic field parallel to the rulings). In the upper layer, the period has two rectangular grooves of width a_{11} and height h_1 (zones 11 and 13, see Fig. 1), and a central neck of the same depth but of width a_{12} (zone 12). The second layer is a rectangular cavity which occupies the whole period, i.e., its width is d and its depth is h_2 (zone 21). The surrounding medium is vacuum. In what follows, both polarizations will be treated simultaneously, denoting by f the z -component of the electric field in the s -case and that of the magnetic field in the p -case.

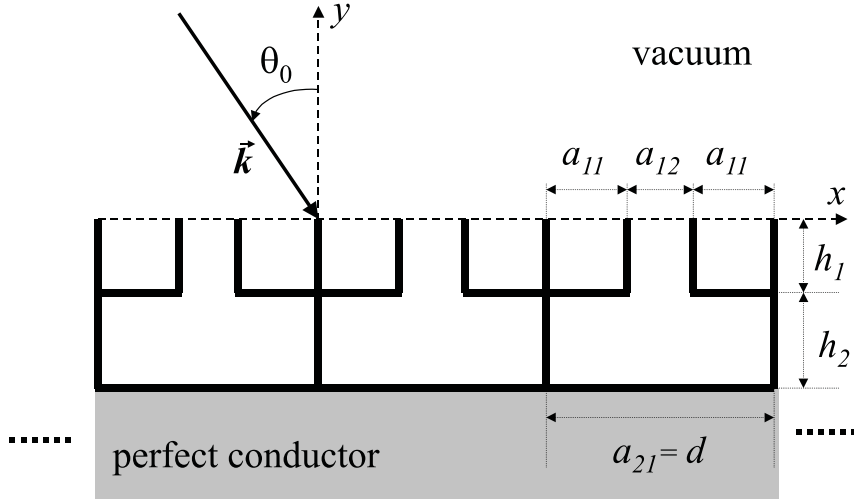


Figure 1: Sketch of the nested diffraction grating.

In an homogeneous medium, the rectangular geometry of the structure allows a separable solution of Helmholtz equation in cartesian coordinates. The modal method consists in expanding the fields inside the corrugations in their own eigenfunctions (modes) that satisfy by themselves the boundary conditions at the sides of the cavities. In the homogeneous region ($y \geq 0$), the total field f is given by:

$$f(x, y) = e^{i(\alpha_0 x - \beta_0 y)} + \sum_{n=-\infty}^{\infty} R_n^q e^{i(\alpha_n x + \beta_n y)} , \quad q = s, p \quad (1)$$

where $\alpha_0 = k \sin \theta_0$, $\beta_0 = k \cos \theta_0$,

$$\alpha_n = k \sin \theta_n = \alpha_0 + n \frac{2\pi}{d} , \quad (2)$$

$$\beta_n = \begin{cases} \sqrt{k^2 - \alpha_n^2} & \text{if } k^2 > \alpha_n^2 \\ i \sqrt{\alpha_n^2 - k^2} & \text{if } k^2 < \alpha_n^2 \end{cases} , \quad (3)$$

$k = 2\pi/\lambda$ is the wave number and R_n^q is the unknown complex amplitude of the n -th diffracted order. The superscript q denotes the polarization case.

As mentioned above, the fields inside the corrugations are expressed in terms of infinite series.

Each zone ij ($ij = 11, 12, 13$ or 21) has its own expansion as follows:

$$f_{ij}(x, y) = \sum_{m=0}^{\infty} u_{ijm}^q(x) w_{ijm}^q(y) , \quad (4)$$

where

$$u_{11m}^q(x) = \begin{cases} \sin \left[\frac{m\pi}{a_{11}} x \right] & \text{for } q = s \\ \cos \left[\frac{m\pi}{a_{11}} x \right] & \text{for } q = p \end{cases} , \quad (5)$$

$$u_{12m}^q(x) = \begin{cases} \sin \left[\frac{m\pi}{a_{12}} (x - a_{11}) \right] & \text{for } q = s \\ \cos \left[\frac{m\pi}{a_{12}} (x - a_{11}) \right] & \text{for } q = p \end{cases} , \quad (6)$$

$$u_{13m}^q(x) = \begin{cases} \sin \left[\frac{m\pi}{a_{11}} (x - (a_{11} + a_{12})) \right] & \text{for } q = s \\ \cos \left[\frac{m\pi}{a_{11}} (x - (a_{11} + a_{12})) \right] & \text{for } q = p \end{cases} , \quad (7)$$

$$u_{21m}^q(x) = \begin{cases} \sin \left[\frac{m\pi}{a_{21}} x \right] & \text{for } q = s \\ \cos \left[\frac{m\pi}{a_{21}} x \right] & \text{for } q = p \end{cases} , \quad (8)$$

$$w_{11m}^q(y) = \begin{cases} C_{11m}^s \sin [\mu_{11m}(y + h_1)] & \text{for } s \text{ polarization} \\ C_{11m}^p \cos [\mu_{11m}(y + h_1)] & \text{for } p \text{ polarization} \end{cases} , \quad (9)$$

$$w_{12m}^q(y) = [A_{12m}^q \sin (\mu_{12m}y) + B_{12m}^q \cos (\mu_{12m}y)] \quad q = s, p , \quad (10)$$

$$w_{13m}^q(y) = \begin{cases} C_{13m}^s \sin [\mu_{11m}(y + h_1)] & \text{for } s \text{ polarization} \\ C_{13m}^p \cos [\mu_{11m}(y + h_1)] & \text{for } p \text{ polarization} \end{cases} , \quad (11)$$

$$w_{21m}^q(y) = \begin{cases} C_{21m}^s \sin [\mu_{21m}(y + h_1 + h_2)] & \text{for } s \text{ polarization} \\ C_{21m}^p \cos [\mu_{21m}(y + h_1 + h_2)] & \text{for } p \text{ polarization} \end{cases} , \quad (12)$$

$$\mu_{ijm} = \begin{cases} \sqrt{k^2 - \left[\frac{m\pi}{a_{ij}} \right]^2} & \text{if } k^2 > \left[\frac{m\pi}{a_{ij}} \right]^2 \\ i \sqrt{\left[\frac{m\pi}{a_{ij}} \right]^2 - k^2} & \text{if } k^2 < \left[\frac{m\pi}{a_{ij}} \right]^2 \end{cases} , \quad (13)$$

and C_{ijm}^q , A_{12m}^q and B_{12m}^q are unknown complex amplitudes. Notice that $u_{ij0}^s(x) = 0$, and then the sum in eq. (4) starts from $m = 1$ in the s -case. The functions $u_{11m}^q(x)$ satisfy the appropriate boundary conditions at $x = 0$ and at $x = a_{11}$, the functions $u_{12m}^q(x)$ satisfy the

boundary conditions at $x = a_{11}$ and at $x = a_{11} + a_{12}$, the functions $u_{13m}^q(x)$ satisfy the boundary conditions at $x = a_{11} + a_{12}$ and at $x = d$, and the functions $u_{21m}^q(x)$ satisfy the boundary conditions at $x = 0$ and at $x = d$. On the other hand, the functions $w_{11m}^q(y)$ and $w_{13m}^q(y)$ satisfy the boundary condition at $y = -h_1$, and the function $w_{21m}^q(y)$ satisfy the boundary condition at $y = -(h_1 + h_2)$, according to the case of polarization.

To solve the problem, the fields in each zone are matched imposing the boundary conditions at the horizontal interfaces $y = -h_1$ and $y = 0$. Then, expression (4) with (8) and (12) is matched at $y = -h_1$ with the field in the central neck of the first layer (zone 12), given by (4) with (6) and (10). For $0 \leq x \leq a_{11}$ and $a_{11} + a_{12} \leq x \leq d$, a null tangential electric field is required. At $y = 0$, the fields in zones 11, 12 and 13 are matched with those in $y \geq 0$, given by eq. (1). All these conditions generate four x -dependent equations, that are projected in appropriate bases (either the modal functions or the plane waves) to give an infinite system of linear equations for the unknown amplitudes, for each polarization case. The explicit expressions of these equations can be found in the Appendix. To find the numerical solution to this problem, we truncate the modal series in (4) and the plane wave expansions in (1), and get a matrix system which is solved by a standard numerical technique of inversion.

3 Numerical results

In this section we analyze the diffraction by nested gratings for s and p polarization, paying particular attention to the surface shape resonances that characterize their electromagnetic response. All the results presented have been checked to satisfy energy conservation within an error less than 10^{-11} . The results for limit cases such as a comb grating ($h_2 \rightarrow 0$) [28] and a bottle-shaped grating ($h_1 \rightarrow 0$) [21] have also been verified. Even though the method was developed for an arbitrary angle of incidence, in all the results presented we consider normal incidence. We analyze the grating response as a function of the depth of the bottom cavities h_2/d and of the width of the neck a_{12}/d (Figs. 2-6) and show the dependence of the behaviour of these structures as a function of the incident wavelength (Figs. 7-8).

In Fig. 2 we plot the specular efficiency versus h_2/d for s polarization, where: $h_1/d = 0.1$, $\lambda/d = 0.65$ and $a_{12}/d = 0.2$ (solid) and 0.4 (dashed). It can be noticed that there are minima in the efficiency curves for certain values of h_2 . These minima are sharper and deeper for the narrower neck of the cavities, and can be associated with surface shape resonances.

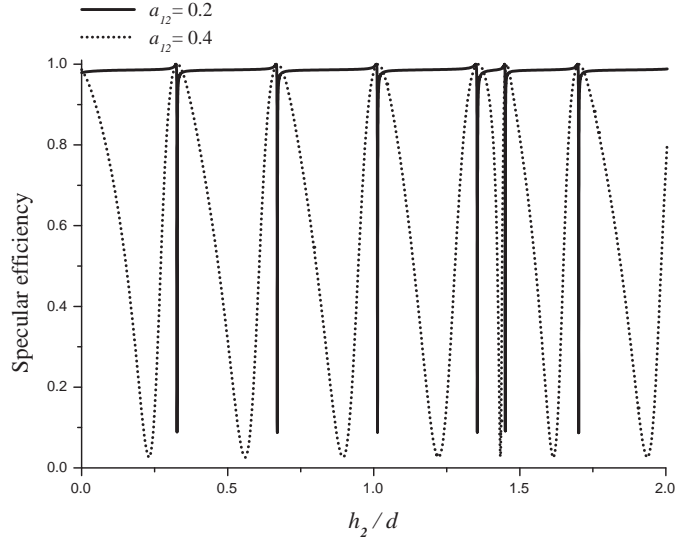


Figure 2: Specular efficiency vs. h_2/d for s polarization. The grating parameters are $h_1/d = 0.1$, $\lambda/d = 0.65$, $\theta_0 = 0^\circ$, $a_{12}/d = 0.2$ (solid) and $a_{12}/d = 0.4$ (dashed)

In Table 1 we compare the resonant depths of the cavities of the nested grating for $\lambda/d = 0.65$ (h_2) with those corresponding to eigenmodes of a closed rectangular waveguide of side d , which are given by

$$\frac{h}{d} = \frac{n}{\sqrt{(2d/\lambda)^2 - m^2}}, m, n \in \mathbb{Z}_{\geq 0}. \quad (14)$$

Notice that the first value of m in (14) is 1 for s -polarization (the x -dependent part of the electric field modes is a pure sine function, and $m = 0$ would imply null field), whereas it is 0 for p -polarization (the x -dependent part of the magnetic field modes is a pure cosine function, and here $m = 0$ implies uniform distribution in the x direction), as it is explicitly shown in eq. (8). Besides, due to the symmetry imposed by the normally incident plane wave, only odd values of m are allowed for s -polarization, and only even values of m for p -polarization. The number of decimal places kept in the tables was determined by the resolution necessary to define correctly each minimum in the efficiency curve. The sharper dips require more decimals than the smooth ones.

The resonant depths of the nested grating are close to those of the closed waveguide obtained by eq. (14), even though the present structure is open. The relationship between the width of the dip, the quality of the resonance and the interior field can be better understood by inspection

m	n	h/d	h_2/d	$pol.$
0	1	0.325	0.037	p
1	1	0.344	0.32675	s
2	2	0.427	0.3349	p
0	2	0.650	0.468	p
1	2	0.683	0.66985	s
2	2	0.855	0.6628	p
0	3	0.975	0.89	p
1	3	1.030	1.01305	s
2	3	1.283	0.9915	p
0	4	1.300	1.29466	p
1	4	1.374	1.35445	s
3	1	1.462	1.45025	s
0	5	1.625	1.339	p
2	4	1.710	1.6342	p
1	5	1.718	1.70125	s
0	6	1.950	1.752	p

Table 1: Resonant depths h/d for a perfectly conducting rectangular waveguide and resonant depths h_2/d found in the nested structure for $a_{12}/d = 0.2$, $h_1/d = 0.1$, for a wavelength $\lambda/d = 0.65$.

of the near field.

In Figs. 3 and 4 we plot the electric field magnitude (relative to the incident field) for different resonant depths of the structure considered in Fig. 2. In all the contour plots presented (Figs. 3, 4, 6 and 8) the black represents maximum intensity, and the gray scale is maintained in all three figures. Figs. 3a to 3f correspond to the resonant configurations for $a_{12}/d = 0.2$, whereas Figs. 4a and 4b correspond to the 1st and 5th resonant cases for $a_{12}/d = 0.4$. It can be observed in Fig. 3, that the contour plots of the inner field in the resonant configurations are similar to the configurations expected for the eigenmodes of a rectangular waveguide. Each one of the figures can be associated with a certain mn mode of the closed waveguide: Fig. 3a. corresponds to the 11 mode, Fig. 3b to the 12, Fig. 3c to the 13, Fig. 3d to the 14, Fig. 3e to the 31, and Fig. 3f to the 15. Besides, the interior field is strongly intensified: the ratio between the maximum value inside and outside the structure varies between 6 (Fig. 3a) and 35 (Fig. 3e) for resonant configurations, whereas out of the resonance the field inside and outside the structure has roughly the same value. Notice that the vertical scale is not maintained in all the figures, and therefore the depth of the cavities look equal although each one corresponds to a different depth. When the neck of the cavities is widened, the quality of the resonances becomes lower,

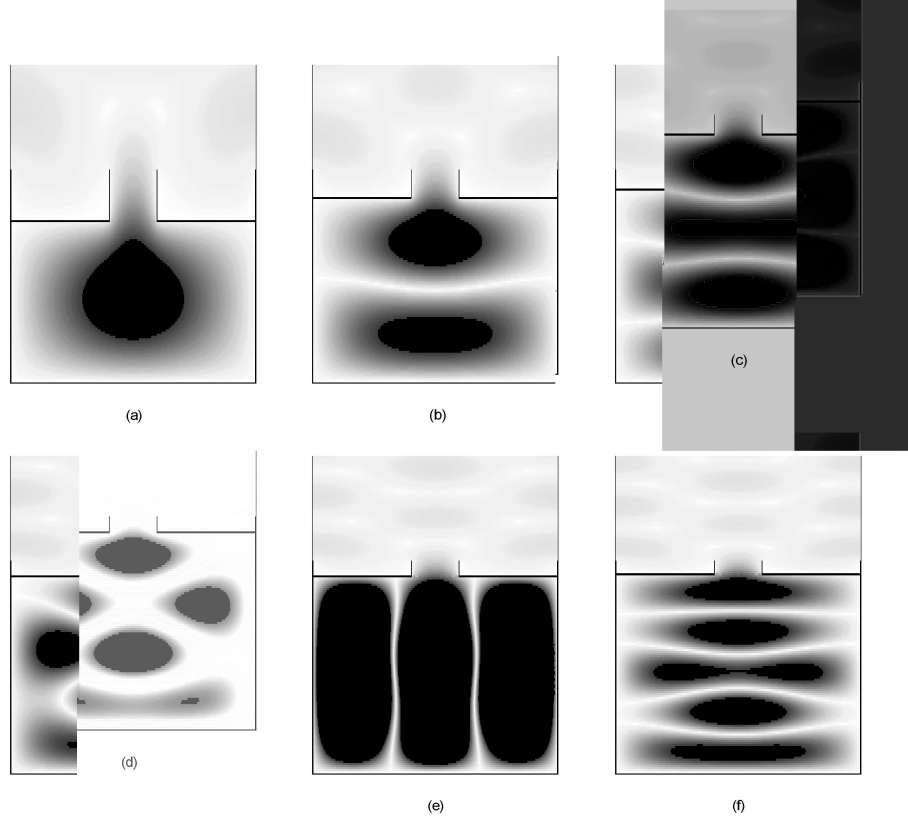


Figure 3: Electric field intensity distribution for a grating with $h_1/d = 0.1$, $a_{12}/d = 0.2$, $\lambda/d = 0.65$, $\theta_0 = 0^\circ$ and s polarization (solid line in Fig. 2): (a) $h_2/d = 0.32675$; (b) $h_2/d = 0.66985$; (c) $h_2/d = 1.01305$; (d) $h_2/d = 1.35445$; (e) $h_2/d = 1.45025$; (f) $h_2/d = 1.70125$.

as observed in the dashed curve of Fig. 2. At the same time, the resonant depths shift to lower values, thus moving further from the predicted depths for the closed waveguide. This behaviour is expected since this structure is less similar to the closed one.

The contour plots of electric field corresponding to this situation are shown in Fig. 4. Fig. 4a corresponds to the first dip ($h_2/d = 0.23$) and Fig. 4b corresponds to the 5th. dip ($h_2/d = 1.4335$). In the first case there is no intensification: the field takes the same values inside and outside the structure. The second case corresponds to the narrower dip of the dashed curve in Fig. 2, and consequently to the better resonance for the range of h_2 considered. In this case there is an intensification, but it is significantly smaller than that of Fig. 3e (for the same resonant mode but $a_{12}/d = 0.2$ instead of 0.4, and h_2 very close to that of the previous case). When the minimum of specular efficiency is better localized, the enhancement of the field increases and so does the quality of the resonance.

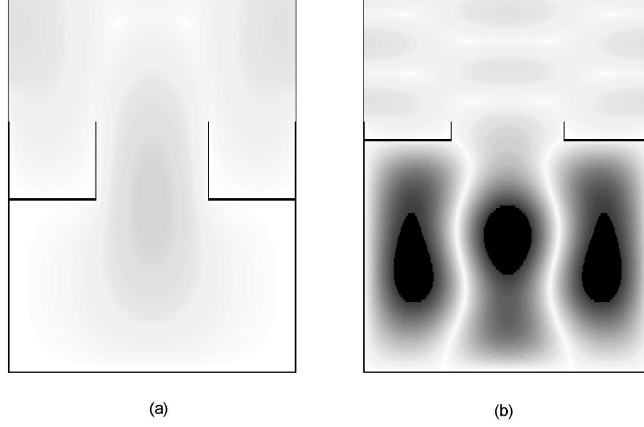


Figure 4: Electric field intensity distribution for a grating with $h_1/d = 0.1$, $a_{12}/d = 0.4$, $\lambda/d = 0.65$, $\theta_0 = 0^\circ$ and s polarization (dashed line in Fig. 2): (a) $h_2/d = 0.23$; (b) $h_2/d = 1.4335$.

The equivalent curve to the solid one in Fig. 2 but for p polarization is shown in Fig. 5. It can be noticed that the minima are not as deep and sharp as in the s -case, and this fact is also reflected in the near field plots of Fig. 6, where we show the magnetic field for the first ($h_2/d = 0.037$) and the 7th. ($h_2/d = 1.29466$) minima of Fig. 5.

Not all the minima for the p -case are located close to those of the closed waveguide, listed in Table 1. This suggests that in general, these minima are not associated with resonances of the lower cavities in the nested grating, as it can be seen, for instance, in Fig. 6a, where we observe that the interior field is not intensified. However, there are certain depths that seem to fulfill the conditions for a resonant mode. This is the case of the 7th dip, whose corresponding magnetic field plot is shown in Fig. 6b. According to Table 1, this dip is located very close to that of the waveguide for the mode 04, and it can be clearly observed in the contour plot that the field distribution is that corresponding to this mode: nearly uniform distribution in the x direction and four half wavelengths in the y direction. Even though this is the most intense case, the intensification ratio is of about 6, roughly the same value of the less intensified mode of s polarization.

We have also analyzed the grating response as a function of the neck width a_{12} , and we have found that for each configuration there is an optimum width for which the specular efficiency has its minimum (not shown). This value arises from a compromise relationship between the

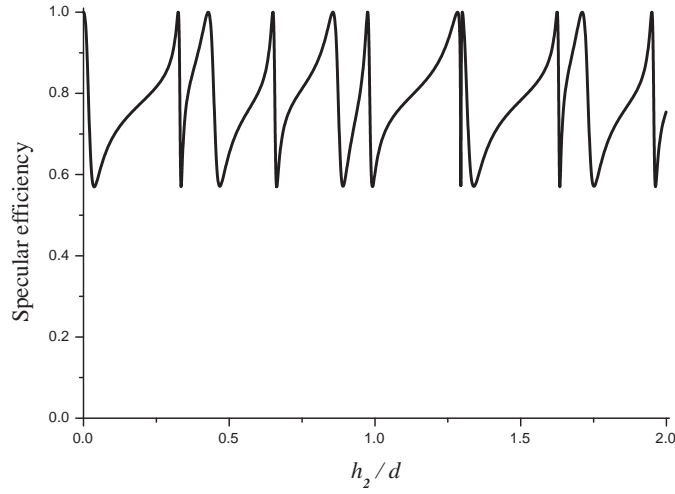


Figure 5: Specular efficiency vs. h_2/d for p polarization. The grating parameters are $h_1/d = 0.1$, $a_{12}/d = 0.2$, $\lambda/d = 0.65$, $\theta_0 = 0^\circ$.

narrowness of the neck and the necessary size of the aperture that allows the field to get into the cavity.

In Figs. 7-8 we explore the response of the nested structure as a function of the wavelength. The specular efficiency for both polarization modes is shown in Fig. 7, for a grating with $h_1/d = 0.1$, $h_2/d = 0.32675$, $a_{12}/d = 0.2$ and $\theta_0 = 0^\circ$. For λ/d greater than one, there is only one diffracted order, and the specular efficiency is equal to unity (not shown). For smaller wavelengths, certain dips start to appear, that become more frequent as $\lambda \rightarrow 0$. It is interesting to notice that there are certain wavelengths in which the efficiency is nearly zero for one polarization, and at the same time it is maximum for the other. For instance, at $\lambda/d = 0.65$ almost all the specularly reflected wave is p -polarized, whereas at $\lambda/d = 0.5$, the reflected wave is s -polarized. Then, this structure behaves as a polarizer for certain wavelengths, which can be varied by properly designing the cavities.

Using eq. (14) to find the resonant wavelengths of a given waveguide, we get the values listed in Table 2, where these values are compared with those corresponding to the dips of the nested grating with $h_1/d = 0.1$ and $a_{12}/d = 0.2$. In the range of wavelengths considered, there are five dips for s polarization and eight for p polarization. As it can be noticed in the efficiency curve, some of them are sharper than others. This suggests that their corresponding resonances

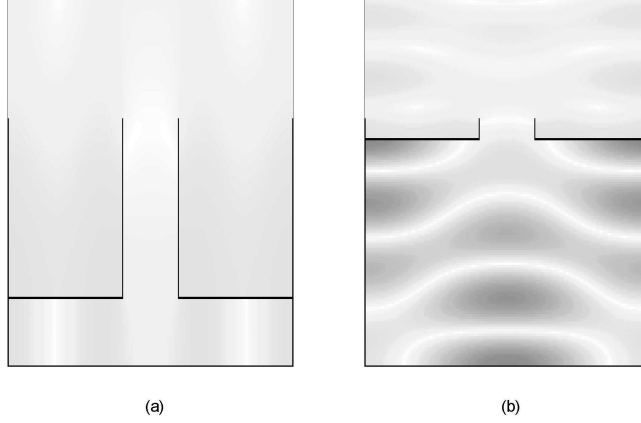


Figure 6: Magnetic field intensity distribution for the grating and incidence conditions of Fig. 5: (a) $h_2/d = 0.037$; (b) $h_2/d = 1.29466$.

are also better, in what concerns to the interior field intensification. This can be confirmed by inspection of the interior field, shown as contour plots in Fig. 8, for p polarization. The figures are ordered by increasing resonant wavelength, and it can be observed that in most of the cases the magnetic field distribution is associated with a resonant mode mn of the rectangular waveguide. For instance, Fig. 8a is the 02 mode, Fig. 8b is the 60 mode, Fig. 8e is the 40 mode, Fig. 8f is the 21 mode, etc. It is evident that the presence of an aperture in the cavity modifies the field distribution of each mode, but most of them can still be identified. An interesting feature found in the wavelength dependence of the response, is the possibility of having modes with $n = 0$. These modes are not allowed in s polarization since they imply null interior field; however, in the p -case, these modes represent an uniform distribution of the field in the y direction. This is the case of the modes 20, 40 and 60, shown in Figs. 8h, 8e and 8b, respectively. In general, the higher intensification is found when the resonant wavelengths are closer to those of the waveguide. Another interesting phenomenon is the splitting of the 41 mode: there are two neighbour dips close to the resonant wavelength predicted for the waveguide, but neither of them is too close (see Table 2). Even though the interior field configurations corresponding to those wavelengths (Figs. 8c and 8d) are different, both can be associated with the 41 mode, but none exhibits a significant intensification. The same effect appears in s polarization for the 51 mode (the corresponding interior field plots are not shown).

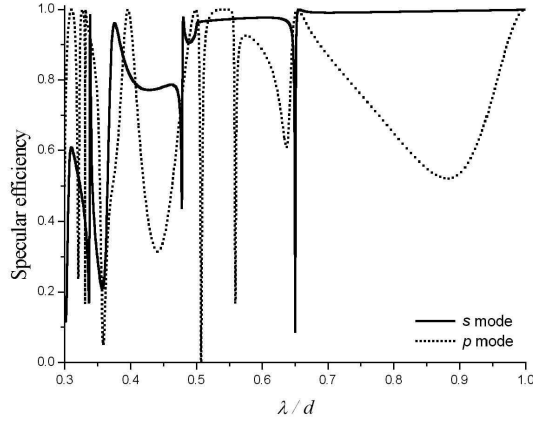


Figure 7: Specular efficiency vs. λ/d for a grating with $h_1/d = 0.1$, $a_{12}/d = 0.2$, $h_2/d = 0.32675$, $\theta_0 = 0^\circ$, for s (solid) and p (dashed) polarization.

In general, the s -surface shape resonances in partially closed cavities are more significant than the p -ones, and this is in agreement with previous reports on multivalued structures [19, 20].

4 Conclusion

The diffraction problem of a nested grating with rectangular cavities was solved for both polarization modes by means of the modal approach. The response of the grating has been analyzed, paying particular attention to the surface shape resonances. It was found that these resonances are stronger for s than for p polarization: the drops in the specular efficiency are sharper and deeper, and the electromagnetic field inside the cavities is significantly intensified. The resonant depths and the contour plots of the near field corresponding to the first modes of the structure are associated with the eigenmodes of a rectangular waveguide.

This study is a first approach to the analysis of the behaviour of nested structures in the presence of electromagnetic waves. The advantages of using this kind of structures as parts of broadband antennas is now being analyzed, not only with the perfectly periodic model but also considering a finite structure and multilayers.

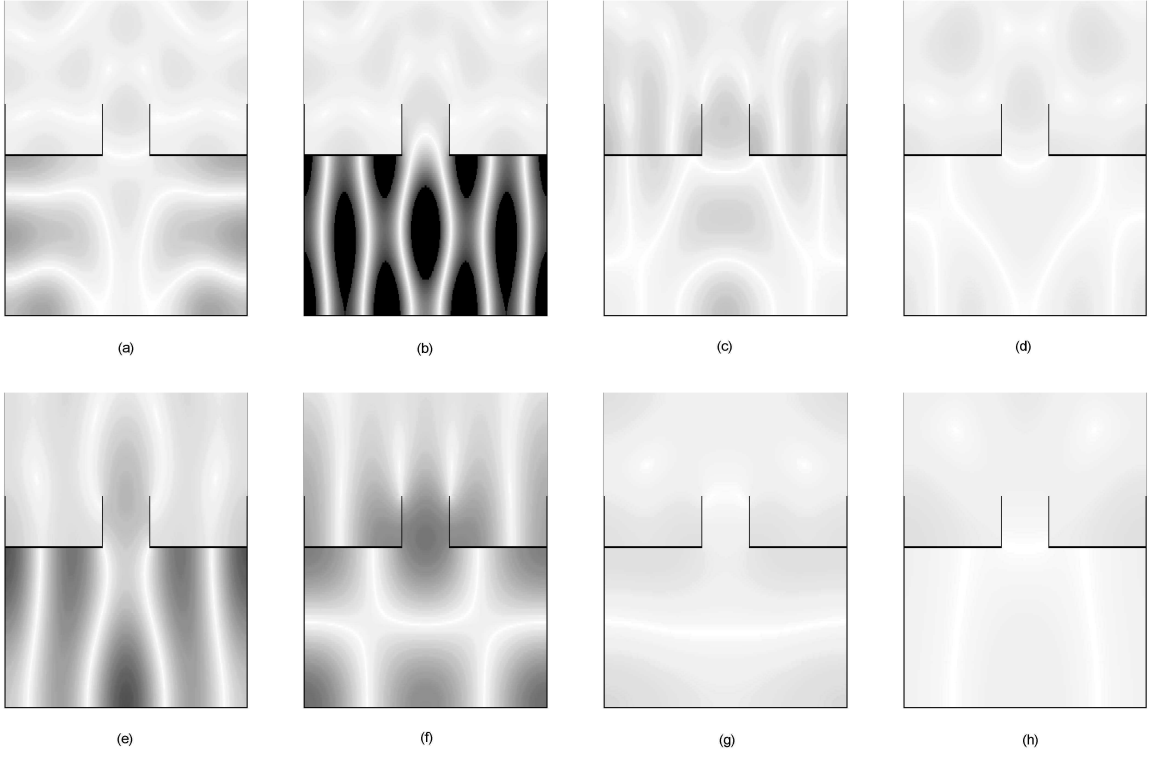


Figure 8: Magnetic field intensity distribution for the grating of Fig.7, for p polarization: (a) $\lambda/d = 0.32099$; (b) $\lambda/d = 0.331$; (c) $\lambda/d = 0.35844$; (d) $\lambda/d = 0.44101$; (e) $\lambda/d = 0.507$; (f) $\lambda/d = 0.55895$; (g) $\lambda/d = 0.63671$; (h) $\lambda/d = 0.88201$.

5 Appendix

By application of the boundary conditions at the horizontal interfaces, we get four x -dependent equations that after appropriate projections generate an infinite system of linear equations for the unknown amplitudes. After a little manipulation of the equations, and making the corresponding truncations, we can summarize the system for each polarization mode as follows.

$$\overline{\overline{M}}^q \overline{A}^q = \overline{\overline{N}}^q \overline{B}^q , \quad (15)$$

$$\overline{\overline{P}}^q \overline{A}^q = \overline{V}^q + \overline{\overline{Q}}^q \overline{\mathcal{R}}^q , \quad (16)$$

$$\overline{\overline{S}}^q \overline{B}^q = \overline{W}^q + \overline{\overline{T}}^q \overline{\mathcal{R}}^q , \quad (17)$$

m	n	λ_w/d	λ_g/d	$pol.$
2	0	1.000	0.88	p
0	1	0.653	0.63671	p
1	1	0.621	0.650035	s
2	1	0.547	0.55895	p
4	0	0.500	0.507	p
3	1	0.466	0.47762	s
4	1	0.397	0.35844-0.44101	p
5	1	0.341	0.33709-0.357	s
6	0	0.333	0.331	p
0	2	0.326	0.32099	p
3	2	0.293	0.30156	s

Table 2: Resonant wavelengths for a perfectly conducting rectangular waveguide λ_w/d and for the nested grating λ_g/d , for $h_2/d = 0.32675$, $a_{12}/d = 0.2$ and $h_1/d = 0.1$.

where

$$M_{nk}^q = \begin{cases} \delta_{nk}(1 + \gamma_{12k}) + \mathcal{U}_{nk}^s(1 - \gamma_{12k}) & \text{for } q = s \\ i[\delta_{nk}(1 - \gamma_{12k}) + \mathcal{U}_{nk}^p(1 + \gamma_{12k})] & \text{for } q = p \end{cases} \quad (18)$$

$$N_{nk}^q = \begin{cases} -i[\delta_{nk}(1 - \gamma_{12k}) + \mathcal{U}_{nk}^s(1 + \gamma_{12k})] & \text{for } q = s \\ \delta_{nk}(1 + \gamma_{12k}) + \mathcal{U}_{nk}^p(1 - \gamma_{12k}) & \text{for } q = p \end{cases} \quad (19)$$

$$P_{nk}^q = \begin{cases} \delta_{nk} & \text{for } q = s \\ \frac{2}{a_{21}\beta_n} e^{i(\mu_{12k}h_1 - \alpha_n a_{11})} I^*(a_{12})_{kn} & \text{for } q = p \end{cases} \quad (20)$$

$$Q_{nk}^q = \begin{cases} \frac{\beta_k}{a_{12}\mu_{12n}} e^{i(\alpha_k a_{11} - \mu_{12n}h_1)} I(a_{12})_{nk} & \text{for } q = s \\ \delta_{nk} + \frac{2}{\beta_n a_{21} a_{11}} [1 + e^{i(\alpha_k - \alpha_n)(a_{11} + a_{12})}] \sum_m \frac{\mu_{11m}}{(1 + \delta_{m0})} \frac{(1 - \gamma_{11m})}{(1 + \gamma_{11m})} I(a_{11})_{mk} I^*(a_{11})_{mn} & \text{for } q = p \end{cases} \quad (21)$$

$$S_{nk}^q = \begin{cases} \frac{2i}{a_{21}} e^{i(\mu_{12k}h_1 - \alpha_n a_{11})} I^*(a_{12})_{kn} & \text{for } q = s \\ \delta_{nk} & \text{for } q = p \end{cases} \quad (22)$$

$$T_{nk}^q = \begin{cases} \delta_{nk} + \frac{2\beta_k}{a_{11}a_{21}} [1 + e^{i(\alpha_k - \alpha_n)(a_{11} + a_{12})}] \sum_m \frac{1}{\mu_{11m}} I(a_{11})_{mk} I^*(a_{11})_{mn} \frac{(1 - \gamma_{11m})}{(1 + \gamma_{11m})} & \text{for } q = s \\ \frac{-i\mu_{12n}}{a_{12}(1 + \delta_{n0})} e^{i(\alpha_k a_{11} - \mu_{12n}h_1)} I(a_{12})_{nk} & \text{for } q = p \end{cases} \quad (23)$$

$$V_n^q = \begin{cases} -Q_{n0}^s & \text{for } q = s \\ Q_{n0}^p - 2\delta_{n0} & \text{for } q = p \end{cases} \quad (24)$$

$$W_n^q = \begin{cases} -T_{n0}^s + 2\delta_{n0} & \text{for } q = s \\ T_{n0}^p & \text{for } q = p \end{cases} \quad (25)$$

$$I(a)_{mk} = \begin{cases} \int_0^a \sin\left(\frac{m\pi}{a}x\right) e^{i\alpha_k x} dx & \text{for } s \text{ polarization} \\ \int_0^a \cos\left(\frac{m\pi}{a}x\right) e^{i\alpha_k x} dx & \text{for } p \text{ polarization} \end{cases} \quad (26)$$

$$\mathcal{U}_{nk}^q = \begin{cases} \frac{4}{a_{12}a_{21}\mu_{12n}} \sum_m J_{km} J_{nm} \mu_{21m} \frac{1+\gamma_{21m}}{1-\gamma_{21m}} & \text{for } q = s \\ \frac{4\mu_{12n}}{a_{12}a_{21}(1+\delta_{n0})} \sum_m J_{km} J_{nm} \frac{1}{\mu_{21m}(1+\delta_{m0})} \frac{1+\gamma_{21m}}{1-\gamma_{21m}} & \text{for } q = p \end{cases} \quad (27)$$

$$J_{mk} = \begin{cases} \int_0^{a_{12}} \sin\left(\frac{m\pi}{a_{12}}x\right) \sin\left(\frac{k\pi}{a_{21}}(x+a_{11})\right) dx & \text{for } s \text{ polarization} \\ \int_0^{a_{12}} \cos\left(\frac{m\pi}{a_{12}}x\right) \cos\left(\frac{k\pi}{a_{21}}(x+a_{11})\right) dx & \text{for } p \text{ polarization} \end{cases} \quad (28)$$

$$\gamma_{ijm} = e^{2i\mu_{ijm}h_i} \quad (29)$$

In the above expressions the unknown modal amplitudes in the neck of the cavities have been redefined:

$$A_m^q = \begin{cases} \frac{1}{2i} A_{12m}^q e^{-i\mu_{12m}h_1} & \text{for } q = s \\ \frac{\mu_{12m}}{2i} A_{12m}^q e^{-i\mu_{12m}h_1} & \text{for } q = p \end{cases} \quad (30)$$

$$B_m^q = \begin{cases} \frac{1}{2i} B_{12m}^q e^{-i\mu_{12m}h_1} & \text{for } q = s \\ \frac{\mu_{12m}}{2i} B_{12m}^q e^{-i\mu_{12m}h_1} & \text{for } q = p \end{cases} \quad (31)$$

and \mathcal{R}^q are the unknown Rayleigh coefficients.

Acknowledgments

This work has been supported by Agencia Nacional de Promoción Científica y Tecnológica (ANPCyT) under grant PICT98-4457, by CONICET (PEI 6216) and by UBA (X150).

References

- [1] Skolnik M: Radar Handbook, Chapter 1, 2nd ed., New York: McGraw, 1990.
- [2] Sievenpiper D, Shaffner J, Loo R, Tangonan G, Ontiveros S, Harold R: A tunable impedance surface performing as a reconfigurable beam steering reflector. IEEE Trans. Antennas Propag. 50 (2002), 384-389.

- [3] Sievenpiper D, Zhang L, Jimenez Broas RF, Alexopoulos NG, Yablonovitch E: High-impedance electromagnetic surfaces with a forbidden frequency band. *IEEE Trans. Antennas Propag.* 47 (1999), 2059-2074.
- [4] Schaffner JH, Sievenpiper D, Loo R, Lee J, Livingston S: A wideband beam switching antenna using RF MEMS switches. *IEEE Antennas and Propagation International Symposium*, vol. 3 (2001), 658-661.
- [5] Gianvittorio JP, Rahmat-Samii Y: Fractal antennas: a novel antenna miniaturization technique and applications. *IEEE Antennas Propag. Magazine* 44 (2002), 20-36.
- [6] Gianvittorio JP, Romeu J, Blanch S, Rahmat-Samii Y: Self-similar prefractal frequency selective surfaces for multiband and dual-polarized applications. *IEEE Trans. Antennas Propag.* 51 (2003), 3088-3096.
- [7] Loui H, Weem JP, Popovic Z: A dual-band dual-polarized nested Vivaldi slot array with multi-level ground plane. *IEEE Trans. Antennas Propag.* 51 (2003), 2168-2175.
- [8] Hessel A, Oliner AA: A new theory of Wood's anomalies on optical gratings. *Appl. Opt.* 4 (1965), 1275-1297.
- [9] Andrewartha JR, Fox JR, Wilson IJ: Resonance anomalies in the lamellar grating. *Optica Acta* 26 (1977), 69-89.
- [10] Wirgin A, Maradudin AA: Resonant enhancement of the electric field in the grooves of bare metallic gratings exposed to S-polarized light. *Phys. Rev. B* 31 (1985), 5573-5576.
- [11] Fantino AN, Grosz SI, Skigin DC: Resonant effect in periodic gratings comprising a finite number of grooves in each period. *Phys. Rev. E* 64 (2001), 016605.
- [12] Grosz SI, Skigin DC, Fantino AN: Resonant effects in compound diffraction gratings: influence of the geometrical parameters of the surface. *Phys. Rev. E* 65 (2002), 056619.
- [13] Skigin DC, Fantino AN, Grosz SI: Phase resonances in compound metallic gratings. *J. Opt. A: Pure Appl. Opt.* 5 (2003), S129-S135.

- [14] Ziolkowski RW, Grant JB: Scattering from cavity-backed apertures: the generalized dual series solution of the concentrically loaded E-pol slit cylinder problem. *IEEE Trans. on Antennas Propag.* 35 (1987), 504-528.
- [15] Maradudin AA, Ryan P, McGurn AR: Shear horizontal acoustic surface shape resonances. *Phys. Rev. B* 38 (1988), 3068-3074.
- [16] Shchegrov AV, Maradudin AA: Acoustic surface shape resonances of circularly symmetric defects on solid surfaces. *Appl. Phys. Lett.* 67 (1995), 3090-3092.
- [17] Maradudin AA, Shchegrov AV, Leskova TA: Resonant scattering of electromagnetic waves from a rectangular groove on a perfectly conducting surface. *Opt. Commun.* 135 (1997), 352-360.
- [18] Valencia CI, Depine RA: Resonant scattering of light by an open cylindrical cavity ruled on a highly conducting flat surface. *Opt. Commun.* 159 (1999), 254-265.
- [19] Valencia CI, Skigin DC, Depine RA: Resonant excitation of the electromagnetic field within a bivalued groove ruled on a highly conducting surface. *Opt. Commun.* 172 (1999), 125-137.
- [20] Skigin DC, Depine RA: Resonant enhancement of the field within a single cavity in a ground plane: comparison for different rectangular shapes. *Phys. Rev. E* 59 (1999), 3661-3668.
- [21] Depine RA, Skigin DC: Resonant modes of a bottle-shaped cavity and their effect in the response of finite and infinite gratings. *Phys. Rev. E* 61 (2000), 4479-4490.
- [22] Zuniga-Segundo A, Mata-Mendez O: Interaction of S-polarized beams with infinitely conducting grooves: enhanced fields and dips in the reflectivity. *Phys. Rev. B* 46 (1992), 536-539.
- [23] Mata-Mendez O, Sumaya-Martinez J: Scattering of TE-polarized waves by a finite grating: giant resonant enhancement of the electric field within the grooves. *J. Opt. Soc. Am. A* 14 (1997), 2203-2211.
- [24] Jovicevic S, Sesnic S: Diffraction of a parallel- and perpendicular- polarized wave from an echelette grating. *J. Opt. Soc. Am.* 62 (1972), 865-877.

- [25] Andrewartha JR, Derrick GH, McPhedran RC: A modal theory solution to diffraction from a grating with semi-circular grooves. *Optica Acta* 28 (1981), 1177-1193.
- [26] Andrewartha JR, Derrick GH, McPhedran RC: A general modal theory for reflection gratings. *Optica Acta* 28 (1981), 1501-1516.
- [27] Li L: Multilayer modal method for diffraction gratings of arbitrary profile, depth and permittivity. *J. Opt. Soc. Am. A* 10 (1993), 2581-2591.
- [28] DeSanto JA: Scattering from a periodic corrugated structure II. Thin comb with hard boundaries. *J. Math. Phys.* 13 (1972), 336-341.